Laidlaw Scholars Research Report

Flexible Solar Cells for Vehicle Surfaces: Tuning Halide Ion Concentration to Offset Bending in Lead-based Perovskite Optoelectronic Properties.

Poline Sidiropoulu[1], **Dr. Claire Barlow**[2] **and Dr. Stephanie Adeyemo**[3]

[1, 2, 3] *University of Cambridge, Newnham College*

This manuscript was compiled on September 29, 2024

Abstract

Flexible and lightweight perovskite solar cells (PSCs) hold significant promise for vehicle surfaces due to their low cost, ease of integration, and potential for enhanced sustainability through recycling. This research investigates the impact of bending curvature (tensile and compressive strain) on the optoelectronic properties of lead-based perovskites, focusing on how halide ion concentration can optimise the offset performance. The study explores the change in bandgap energy, charge carrier mobility and thermal conductivity in response to varying compressive and tensile strains. Findings indicate that compressive strain enhances charge mobility and thermal conductivity by reducing electron-phonon coupling, while tensile strain has the opposite effect, degrading performance and stability. However, the direction of strain application remains the most important factor due to the anisotropic nature of perovskites. The models in the study demonstrate how bending curvature due to vehicle surfaces affects the optoelectronic properties of perovskites. These insights offer pathways for improving the mechanical reliability and efficiency of PSCs, particularly for applications on non-flat surfaces, by leveraging strain engineering and compositional tuning.

Keywords: *perovskite, curvature, optoelectronics, computational modelling, strain, charge carrier mobility, thermal conductivity, bandgap energy, halides*

Corresponding author: Poline Sidiropoulu. *E-mail address:* ps972@cam.ac.uk

Contents

1. Introduction

About 85% of the world's energy comes from non-renewable fossil fuels, such as oil, coal, and natural gas, which is one of the key contributors to climate change [20]. The development of renewable energy sources is now of utmost importance. Pioneering the future of clean and renewable energy, solar cells are setting new benchmarks while ensuring environmental sustainability.

Flexible halide perovskites are a new class of solar cell materials that can be processed at low cost yet exhibit excellent optoelectronic properties with exceptional efficiencies rivalling commercially available technologies such as silicon [32], [49]. Interestingly, the intrinsic mechanical flexibility achievable in halide perovskites enables them to be utilised in lightweight and flexible solar cells for conformable applications, for example, adapting them to the dynamic contours of electric vehicles (EVs) to develop future green and sustainable transportation.

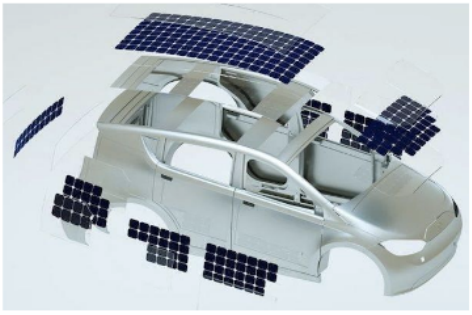

Figure 1. Solar cells for a vehicle's surface [1].

The perovskite layer is easy to recycle, and the substrates can be reused; this makes PSC panels more sustainable from the circular economy point of view and can be used for multiple car surfaces [48], [53]. However, to create flexible and bendable perovskite solar cells, it is important to assess the impact of the bending curvature on the material's performance. Hence, the key goal of this research is to investigate how the application of curvature affects the optoelectronic properties of lead-based perovskites and whether these properties can be optimized by tuning halide ion concentration, and ultimately create simulations to visually describe this.

2. Background Theory

2.1. Introducing Perovskites

Perovskites (PVKs) are characterized by their general formula ABX_3, where 'A' represents a cation, 'B' is typically a metal cation, and 'X' is a halide anion. The crystal structure of perovskites is advantageous for

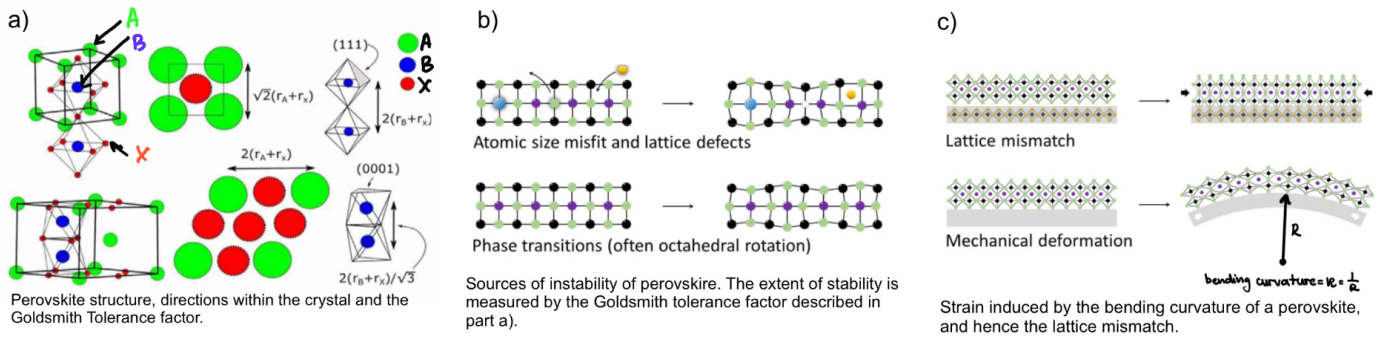

Figure 2. Introducing perovskite structure [20], [66].

solar cell applications due to the ease with which its optoelectronic properties can be changed by tuning halide ion concentration [69].

This is because optoelectronic properties depend on the phase of the PVK, which in turn depends on the stability of the structure determined by its atoms [12], [44], as distinct atoms induce varying internal strain. This affects the stability and sustainability of the whole structure which is assessed by the Goldsmith tolerance factor [58], [66] now adjusted specifically to perovskites [24].

2.2. PVK optoelectronics

The optoelectronic properties of a solar cell semiconductor layer (perovskite) define its performance. We discuss bendgap energy, charge carrier mobility and thermal conductivity as these properties provide a comprehensive outlook on the performance of a solar cell [17].

The bandgap energy determines the spectrum of sunlight it can absorb, hence the open-circuit voltage. Due to the sunlight spectrum distribution, it is best when $Eg = 1.34eV$. *Charge carriers* in perovskites are the electrons and holes created when sunlight excites the electrons in the material. Their ability to move freely through the material is mobility and a higher mobility allows for a better generation of current. *Thermal conductivity* [55] affects the stability of a perovskite, and is typically low, which can be problematic under high solar irradiation as it leads to faster degradation [54].

2.3. Perovskite Solar cells (PSCs) Performance

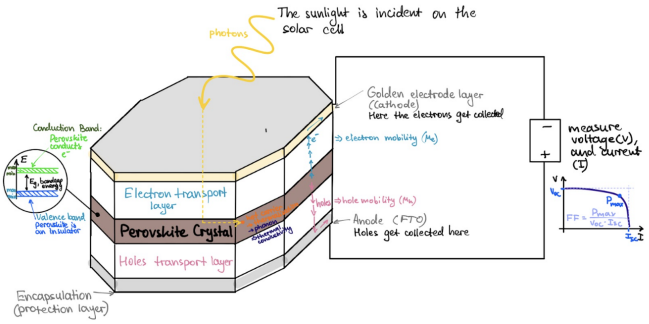

Figure 3. Explaining significance of selected optoelectronic properties

The performance of the solar cell depends on all layers and is measured by the power conversion efficiency:

$$\text{PCE} = \frac{P_{\text{out}}}{P_{\text{solar}}} \times 100\% = \frac{FF \times I_{sc} \times V_{oc}}{P_{\text{solar}}} \times 100\%$$

FF is the fill factor, it describes how "squary" the IV-curve is [44].

2.4. Mechanical properties of perovskites

Mechanical properties that govern the deformation of PVK during bending are Young's modulus, Poisson's ratio and hardness. These are influenced by the compositional nature of the provskite [1]: the Pb-X bond strengths, the packing density, and the chemical bonding.

Perovskires are anisotropic [1], [44]. This leads to directional variation in optoelectronic properties due to differing effective elastic constants and wavevectors. Measuring them in one direction is incomplete, as optoelectronic properties vary hugely across major crystallographic directions.

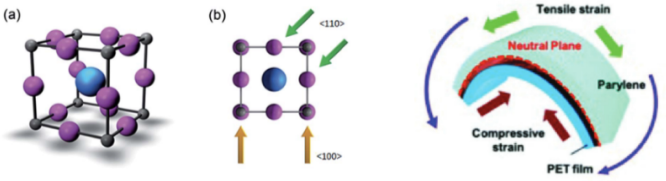

(a) Different strain directions [1] **(b)** Bent PVK on a substrate [20]

Figure 4. Mechanical properties of a perovskite.

Indentation along the (100) directions aligns with the Pb-X-Pb inorganic bonds, providing strong resistance. Conversely, stress along the (110) direction moves the indenter against a less rigid inorganic bond, causing greater displacement. When we bend a perovskite, a curvature is applied and can be expressed using strain: $\varepsilon = \kappa \cdot y$

Films exhibit a vertical gradient of strains (which is in agreement with the bending theory) [21], [22], [25], [72]. Due to Poisson's effect, the applied curvature generates opposing strains in directions perpendicular to the uniaxial strain as shown in Figure 4 [24].

2.5. Material choice and initial strain calculations

Lead-based perovskites ($CsPbBr_xI_{3-x}$ and $CH_3NH_3Br_xI_{3-x}$) were selected for their optimal optoelectronic properties [54]. Br and I enhance stability [36], Cs improves efficiency [35], and NH_3 relaxes strain [8], [14], [10].

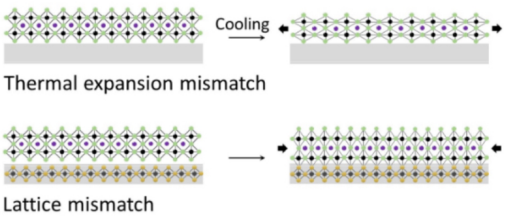

Figure 5. Strain induced by the substrate.

Originally, the experiment would involve thin films, but we looked at single crystals instead [17]. They show enhanced carrier transport and stability due to lower defect concentration [43]. Even though thin films are twice as flexible as single crystals, they have ion migration [4], increasing the instability especially under thermal strain [22].

PET and PEN substrates [49], [51] were chosen due to their high light transmission, conductivity, and coefficients of thermal expansion compatibility, which minimised cooling-induces stress [7]. Substrates can act as a barrier to oxidation or moisture [32], and further encapsulation with a PEI layer on the top creates an even distribution of stresses [6]. PET and PEN allow surface roughness to avoid electrical short-circuiting in the device [45]. These also prevent wrinkling and delamination [48].

Matlab was used to assess the impact of temperature on the distribution of thermal-induced strains within the perovskite and its substrate layers (i.e. the initial strains). Partial differential equations (Matlab PDE) were used for the temperature distribution problem, and Finite Element Analysis (Matlab FEA) to estimate the strains. The first subfigure in Figure 6 is by Yinan Jiao and provides a general outlook on this [44].

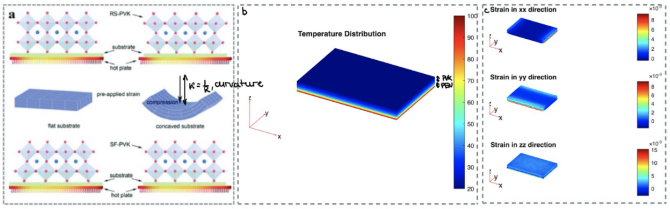

A) Scheme of formation of residual strains within a perovskite crystallized on a substrate. Copyright 2022. The Royal Society of Chemistry, B) My Matlab PDE model for assessing the temperature distribution within the perovskite and the film C) My Matlab FEA model to assess the strain distribution within the perovskite and the substrate

Figure 6. Thermal-induced strains and temperature distribution.

The initial idea for the bending setup was to 3D-print semicircles of a fixed radius, but we used 3-point bend-test from Stranks group within the Department of Chemical Engineering and Biotechnology.

Background theory summary

Bending a perovskite induces strain across all planes, impacting its optoelectronic properties: bandgap energy, charge carrier mobility, and thermal conductivity. To minimize initial strain, we selected an optimal perovskite and substrate.

3. Methodology

3.1. XRD

Due to asymmetry and the sizes of the atoms involved in the crystal lattice, PVK has an initial (internal) strain in PVK even before bending [18], [24], [54]. Hence, we use XRD to identify it [36], [37].

The information from different depths from the surface to bulk is obtained by changing the incident angle: the larger the incident angle, the deeper the X-ray penetrates from the surface.

Under tensile strain, diffraction peaks drifted towards lower values, so the slope is negative. However, compressive strain shifts diffraction peaks towards a larger angle so the slope is positive [12]. Strain is usually extracted from Bragg peak positions and Bragg peak shapes:

$n\lambda = 2d\sin\theta \quad \Rightarrow \quad \varepsilon = \frac{d_{\text{strained}} - d_{\text{unstrained}}}{d_{\text{unstrained}}} \times 100\%$, where d_{strained} is the lattice spacing of the strained crystal, and $d_{\text{unstrained}}$ is that of the unstrained crystal.

Using Williamson-Hall analysis [31], [37]: $\beta\cos\theta = \frac{K\lambda}{D} + 4\varepsilon\sin\theta$, so scanning a beam of small spot size across a sample can produce a map of tensile/compressive strain.

3.2. Terahertz, THz

THz, unlike Hall effect measurement, can be used to non-destructively analyse samples. This is crucial when analysing lead-based perovskites due to their instability for some atomic ratios[75]. Thz full strength lies in its ability to summarise all phenomena happening within a perovskite into a comprehensive picture of charge transport.

In perovskites, phonons affect both thermal conductivity and electronic properties because these quasiparticles interact with charge carriers [39]. Additionally, polarons are formed when atoms surrounding a free carrier are displaced due to electrostatic attraction to the carrier. This interaction creates a potential well around the carrier, limiting its mobility. As the formation of a polaron requires the distortion of the lattice, it results in a signature within the phonon spectrum in the THz regime [74]. At room temperature, this can have a significant effect on even the conductivity.

The LO phonon frequency increases as the halogen X is changed from I to Br to Cl (from heavier to light atoms) [26], which lies in the THz part of the spectrum. Alternatively, the breadth of a PL peak reflects the thermal distribution of carriers and the linewidth is determined by strong electron-phonon interactions [26], [76].

For charge carrier mobility and thermal conductivity two key measurements are: Optical-Pump THz Probe (OPTP) [26] and Time-Resolved THz Spectroscopy (TRTS).

3.3. Hyperspectral imaging

Mechanical bending reduces defects, as evidenced by the increased PL intensity [4], [44], [65], [71]. When the halide ion concentrations are changed, carrier diffusion and the effect of luminescence reabsorption [64] cause the redshift.

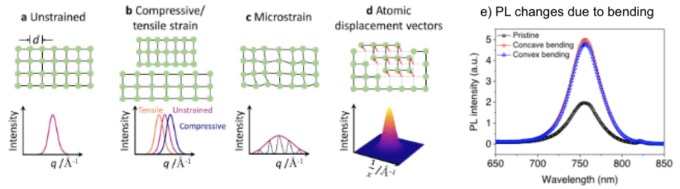

Figure 7. Strain and halide ion concentration impact on PL data.

3.4. Controlling the variables

- The thickness and volume [6], [66] of the PVK as it creates a bandgap gradient:
  - Charge carrier transfer rate decreases with an increase in perovskite thickness [34].
  - When working with very thin films (< 100 nm), surface imperfections can dominate charge carrier dynamics [64].
- The atmosphere during the experiment [64]:
  - Exposing PVK to dry air/ oxygen/ water during measurement can increase the PL intensity and lifetime [24].
- The light conditions during the experiment [64]:
  - Light can prolong PL lifetime and increase its intensity.
  - For mixed halide perovskites, photoinduced phase segregation can shift the PL emission peak.
  - Perovskite solar cells (PSCs) usually operate under low irradiation, but time-resolved spectroscopy often uses higher intensities and pulsed excitation, hence changing the predicted circuit parameters [64].

3.5. Simulations

- Quantum Espresso for DFT calculations;
- Looked into Seftos and SCAPs for solar cell modelling [9], [33], and VESTA for modelling perovskite crystals [26];
- CAD for designing the vehicle surface, and Modelo**41** to work with existing designs;
- Python (Numpy, Scipy, OpenCV) for data analysis and Matlab for simulations, some inspired by Chinedu E. Ekuma, 2024 [16]:

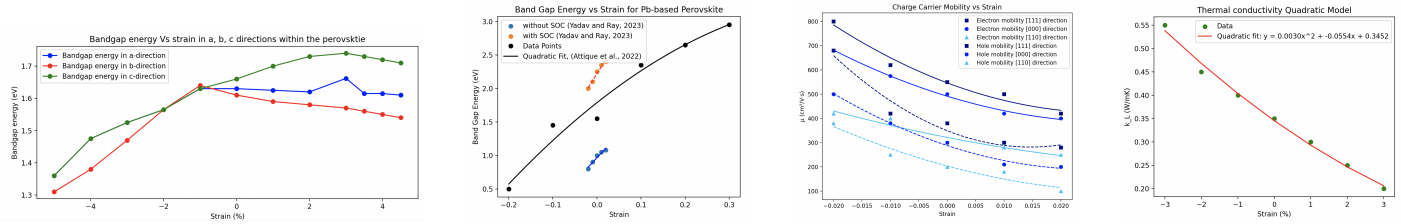

(a) Measured Eg. **(b)** Calculated Eg. **(c)** Electron/ hole mobility. **(d)** Thermal conductivity.

Figure 8. The impact of strain on bandgap energy, charge carrier mobility, and thermal conductivity [23], [55], [60]

- Perovskene Github repository [62];
- IonMonger for solar cells modelling [46], [63];
- My Github repository with simulations and data analysis.

3.6. Comments on uncertainty

1. An exponential fit is a common approach for PL measurements, but not a fixed approach.
2. Differences between partially assembled devices and fully assembled architectures arise from built-in electric fields and unbalanced carrier extraction in full assemblies.
3. Grain boundaries with unique chemical compositions, mean that single crystals will behave differently from the bulk [17].
   a. PL intensities and lifetimes are lower at grain boundaries.
   b. A larger spread in crystal misorientation can lower PL intensity, indicating that crystal mismatch sites [21] can also act as recombination centers.
   c. Laterally oriented grain boundaries can reduce μ_h, but have less impact on μ_e, hence the asymmetries in vertical/horizontal charge transport within the PVK.
   d. The granular structure of perovskite layers can lead to trap or defect states due to crystal strain/element vacancies, such as dangling bonds [45]. These defects cause charge carrier recombination, so efficiency is lost in devices [64].

Methodology summary

PL measurements on existing perovskites to find bandgap. Looked into THz to find carrier properties on other samples (InP nanowires). Matlab for simulations, but Python for data work.

4. Strain engineering

Strain engineering is novel approach to that improves the performance and stability of perovskite solar cells by varying strain until a PVK reaches the needed parameter [6, 12, 52, 58, 60].

4.1. Bandgap energy changes

The band gap of $CsPbI_3$ can be tuned from 1.03 to 2.14 eV by varying strain from -5% to 5%. At a strain of -3%, $CsPbI_3$ achieves an optimal band gap of 1.34 eV, aligning with the optimal range for photovoltaic performance according to the Shockley–Queisser theory [61].

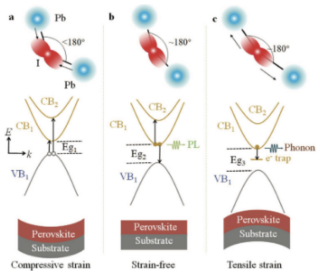

Figure 9. Strain impact on Bandgap energy and band structure [12], [44].

The positions of the Conduction Band Minimum and Valence Band Maximum shift under strain. Tensile strain shifts them downward (decreasing E_g), while compressive shifts them upward (increasing E_g) [13] because of the changes in the lattice parameters hence the wavevectors Figure 8 (b).

The band gap of $CH_3NH_3PbI_3$ oscillates as compressive strain increases due to nonlinear structural deformations and phase transitions under large strains (different from other semiconductors) [67].

Using Figure 6 we can construct a best fit line to correlate the bending-induced strain with perovskite E_g [6, 16, 27, 61]:

$$E_g(\varepsilon) = -2.054\varepsilon^2 + 8.184\varepsilon - 4.528 \quad \text{(Scipy best fit line)}$$

In a and b directions the decrease in E_g is identically related to the affection of the VBM and CBM by strains [4]. In the c direction, the changes in E_g are anisotropic since I-Pb-I bond is flexible [69], Figure 8 (a). The crystals change their equilibrium positions, and this displacement generates a distortion of the crystal lattice. By increasing strain, octahedral tilt becomes more important because of stabilisation of Pb 6s-I 5p* and I 5p states near the VBM [10, 37, 70].

Ultimately, the best-fit lines are close on Figure 8 (b), with differences explained by DFT calculations with and without SOC. Experimental results fall in between, supporting this conclusion.

4.2. Charge mobility changes

Compressive strain increases hole mobilityμ_h due to decreasing the hole effective mass [23, 51, 70]. Tensile strain increases the current density under the same applied V [6, 21], which is indicative of increased electron mobility μ_e.

For $CsPbI_3$ and $CsPbBr_3$ μ_e, increases with compressive strain and decreases with tensile strength [18, 52]. For example, μ_e increases from 11 to 143 $cm^2\ V^{-1}s^{-1}$ under 13% compression [39].

Compressive strain raises VBM more than the CBM due to stronger interactions between Pb 6s and I 5p orbitals. VBM upward shift improves its energetic alignment with the Au contact's Fermi level through decreasing the physical distance between the layers. This increases photocurrent and carrier mobility, improving charge transfer at the perovskite/HTL interface [31, 37].

[111] direction: $\mu_h = -6700 \cdot \varepsilon + 616$, and $\mu_e = -6600 \cdot \varepsilon + 650$
[100] direction: $\mu_h = -5000 \cdot \varepsilon + 400$, and $\mu_e = -6000 \cdot \varepsilon + 420$
[110] direction: $\mu_h = -5000 \cdot \varepsilon + 300$, and $\mu_e = -5000 \cdot \varepsilon + 340$

4.3. Thermal conductivity changes

Thermal conductivity $= \kappa_L = \frac{1}{3} C_v v_s l$ where C_v is the specific heat capacity per unit volume (not affected by strain), v_s is the speed of sound (phonon velocity) in the material, and l is the mean free path of phonons [37]. Also, $l \sim \frac{1}{\text{density of scattering centres (defects/other atoms)}}$

Phonons travel within the perovskite and their velocity is influenced by the strength of chemical bonds - stronger bonds lead to faster phonon group velocities. Compressive strain increases them due to the steeper dispersion curves resulting from the spread-out phonon bands. Opposite happens under tensile strength.

The mean free path is the average distance a phonon can travel before it collides with another phonon, a defect, or a boundary. A

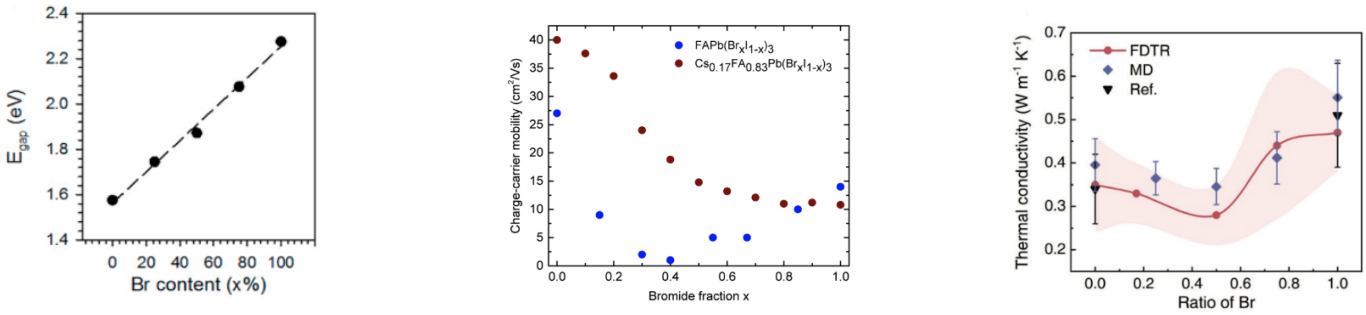

(a) Bandgap energy. **(b)** Charge carrier mobility. **(c)** Thermal conductivity.

Figure 10. The impact of halide ion concentration on the optoelectronic properties of a perovskite.

longer mean free path allows for better heat transfer [11]. Compressive strain increases the density of atoms in a given volume, which would tend to decrease the mean free path. Tensile strain decreases the density, increasing the mean free path.

Therefore, compressive strain generally increases thermal conductivity in as it brings atoms closer together, strengthening their bonds. Fewer defects/ irregularities increase the mean free path [5]. It also enhances the overlap of atomic orbitals, increasing and conductivity. While tensile strain decreases the thermal conductivity because it weakens the bonds between atoms and localises the charges [11] resulting in slower phonon group velocities. The stretched structure might introduce more defects or irregularities, potentially decreasing the mean free path. [11], [37], [39] (VESTA [79]).

We can now extract the data from graph c) on Figure 9:

$$\kappa_L = 0.0030 \cdot strain^2 - 0.0554 \cdot strain + 0.3452$$

However, κ_L may be unchanged under small strains, as most phonons responsible for it have l of less than 100 nm [26]

4.4. Thin films and strain engineering

- Compressive strain lifts the VBM more than the CBM, improving carrier mobility and energy alignment with the HTL, while tensile strain lowers the VBM, creating an unfavorable gradient for hole extraction and leading to defects [44].
- Bulk conductivity of PVK decreases under tensile strain, but increases under compressive strain (DFT calculations) [12].
- Compressive strain stabilizes a perovskite, while tensile strain accelerates its degradation [37].
- Small compressive strain (|2.5%|) does not significantly affect PVK optoelectronic properties [71].
- Tensile strain in the lattice increases ion migration, while compressive strain raises the migration barrier by distorting the octahedra and shortening the Pb-I bond, preventing I ions from leaving the Pb site [12].

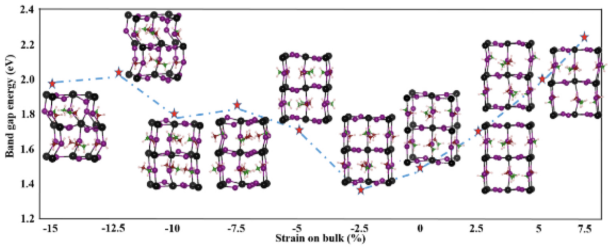

Figure 11. Bulk bandgap energy changes due to strain [20].

In PSC devices, lattice mismatches occur at the interfaces of the sandwich-like structure, where the $CH_3NH_3PbI_3$ perovskite layer is placed between the HTL and window layers as shown in figure 11. Orientations of $CH_3NH_3^+$ molecules of the upper layer are opposite to those of the bottom layer [38], [67]. Such as, $\varepsilon_{\text{tensile}}$ decreases activation energy for ion migration, which accelerates the degradation of perovskite, while $\varepsilon_{\text{compressive}}$ increases activation energy, thus suppressing such degradation [51].

Summary of strain engineering

Strain alters the optoelectronic properties of perovskites, often negatively impacting solar cell performance, making compensation necessary. The direction of strain plays a critical role in these changes due to the anisotropic nature of perovskites.

5. Compositional engineering

Compositional engineering is the change in the atomic formula of a perovskite to tune its optoelectronic properties.

5.1. Tuning bandgap energy

Changing the B or X site anion allows for direct tuning of the bandgap energy, while A-site atoms influence Eg indirectly through symmetry. Halide anions differ in atomic radii and electronegativities, with electronegativity decreasing and atomic radius increasing down the group [19, 27, 28]. This affects the orbital overlap between metal and halide ions, influencing the conduction and valence band energies. Substituting chlorine with bromine or iodine leads to a redshift in the absorption spectrum, indicating a narrowed bandgap. [29, 58]

Hence, extracting the data from the graph:

$$E_g = 0.0075 \times (\text{Br content}) + 1.55$$

5.2. Tuning charge carrier mobility

From the Figure 10 (b) we can derive the relationship between charge carrier mobility and halide ion concentration for 2 PVKs [26]:

$$\mu_{\text{FA}}(x) = 22.32x^2 - 4.46x + 8.21$$
$$\mu_{\text{CsFA}}(x) = 5.84 \cdot 10^{-5}x^2 - 31.43x + 40.71$$

The relationships stem from Frohlich interactions (i.e. the interactions between the electrons and phonons) which are stronger in $APbBr_3$ than in $APbI_3$ (for A = MA, FA) due to the higher ionicity of the Pb-Br bond, which limits μ [60].

5.3. Tuning thermal conductivity

Thermal conductivity of $MAPb(Br_{1-x}I_x)_3$ can be changed by halide alloying: $0.27 \pm 0.07\,(x = 0.5)$ to $0.47 \pm 0.09\,\text{Wm}^{-1}\text{K}^{-1}\,(x = 1)$.

This is achieved by increasing phonon scattering. Additionally, the diffusion of MA+ cations in the octahedra cage acts as an additional thermal transport channel in hybrid perovskites [37] (Figure 10 (c)). However, this contribution may be small at room temperature (RT).

$MAPbX_3$ single crystals show increasing average thermal conductivity as the atomic number of the halide decreases [37]. Heavier halide ions result in lower elastic stiffness in the Pb-X lattice, which reduces v_s, decreasing thermal conductivity (λ). The more significant the scattering (common in heavier halide systems), the shorter the phonon mean free path, further reducing λ.

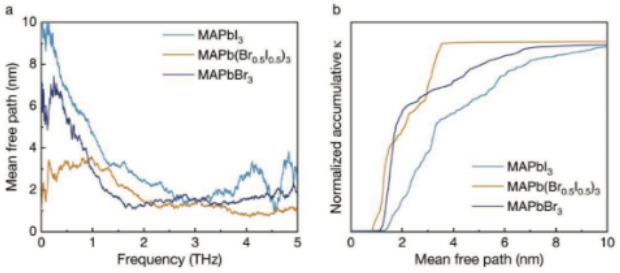

Figure 12. Mean free path as a function of frequency and halide ion concentration and thermal conductivity as a function of mean free path [40].

MD simulations show that the reduction of thermal conductivity of PVK is mainly attributed to the suppression of the mean free paths of the low-frequency phonons, which results from the strong phonon scatterings caused by alloying [40].

FDTR Fit: $y = 1.4552x^4 - 2.0449x^3 + 1.0599x^2 - 0.3475x + 0.3522$

MD Fit: $y = 1.3035x^4 - 1.7495x^3 + 0.8938x^2 - 0.2932x + 0.3409$

Thermal conductivity of the PVK reaches its minimum at a Br ratio of 0.5 [40]. In the tetragonal phase of $MAPbI_3$ at room temperature, the low thermal conductivity of 0.59 W/m·K is due to the reduced phonon group velocity, which is a result of low elastic stiffness and anharmonicity. However, the pseudo-cubic phase exhibits a significantly higher predicted thermal conductivity of 1.80 W/m·K at 57°C, attributed to longer phonon lifetimes and an increased phonon group velocity [11].

Summary of Compositional engineering

When changing the chemical composition of a perovskite we induce internal strain due to the different sizes of atoms. This in turn can offset the external strain caused by the bending curvature, allowing us to maximise the efficiency of a perovskite solar cell and the optoelectronic properties of the perovskite material.

6. Bending and Solar Cells

Perovskite is one of the solar cell's layers, so it is crucial to look into the how bending curvature affects the overall performance (PCE) of an SC. Bending can be convex and concave, hence inducing tensile and compressive strains on different sides of the material [6].

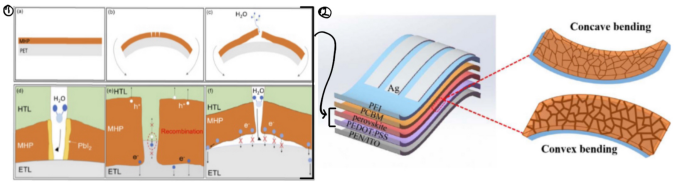

Figure 13. Bending a solar cell [42], [47].

Although convex bending smooths the perovskite interface, the PV performance degradation is likely unrelated to interface damage [70]. F-PSCs exhibit better mechanical stability with concave bending but the film's roughness increases, increasing leakage current [47]. The conductivity decrease of PVK film is responsible for the increased shunt resistances, hence poorer mechanical stability after convex bending (as shown in Figure 14). Ultimately, during bending grain boundary cracks allow moisture to penetrate and decompose MHPs, reducing FF. However, the photoexcited electrons become dominant with compressive strain. So, the PCE increases [20].

Compressive strain increases the current for a given value of applied voltage. On the contrary, tensile strain always reduces charge transport.

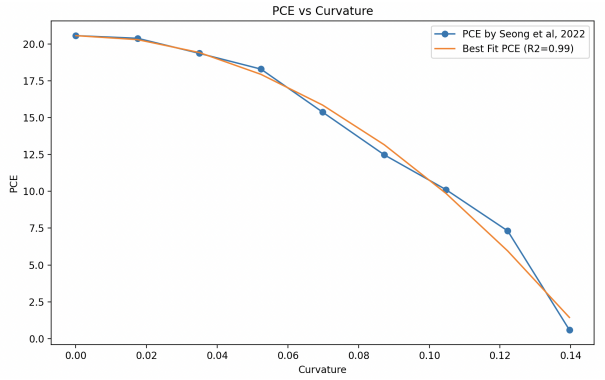

Figure 14. PCE as a function of curvature.

This figure was inspired by [51], and from the graph:

$$PCE, \% = -994.9676\kappa^2 + 1.9772\kappa + 20.5585$$

The degradation of photovoltaic performance under convex bending is mainly caused by the FF reduction [42], [47], [51]. The FF shows a linear reduction with decreasing the bending radius to 74 percent of the initial value after bending at r = 3 mm. As a result, the PCE exhibits good stability within a bending radius of 5 mm, but decreases quickly at smaller curvature radii. Whereas the device with convex bending, the Voc has an increasing trend with decreasing bending radius. The Js shows better tolerance against bending curvature. As we can see, concave bending gives better mechanical stability. [22]

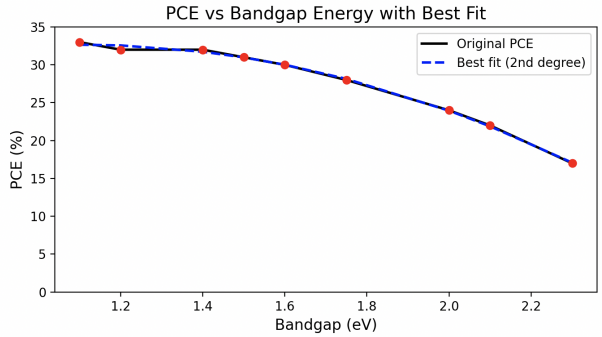

Figure 15. PCE as a function of bandgap energy.

The optoelectronic properties of a solar cell affect its efficiency too:

$$E_g(\varepsilon) = -2.054\varepsilon^2 + 8.184\varepsilon - 4.528 = -2.054(\kappa \cdot y)^2 + 8.184(\kappa \cdot y) - 4.528$$

From the graph [42], [57]: $PCE = -10.91E_g^2 + 27.14E_g + 10.85$

Therefore, the PCE of a solar cell can be expressed as both the function of the optoelectronic properties of a solar cell, and the strain that affects them. Therefore, to offset it, we can tune the halide ion concentration, so data taken by Helal Miah et al, 2024 was used [58].

Now, we can plot the best fit on one graph to extrapolate further

correlation between bending, halide ion concentration and PCE.

$$PCE = 32.7 \cdot HalideConcentration^2 + 33.4 \cdot E_{bandgap}^2 - 65.6 \cdot HalideConcentration \cdot E_{bandgap} - 6.11 \cdot HalideConcentration + 2.7 \cdot E_{bandgap} + 3.99 \quad (1)$$

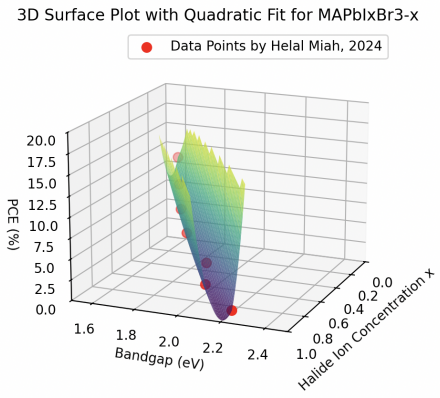

Figure 16. PCE as a function of E_g, and halide ion concentration.

7. Experimental results

The results were very close to the theoretical predictions. Additionally, close to the boundaries of the single crystal perovskite we found photo-brightening too.

7.1. PL measurements (for bandgap energy)

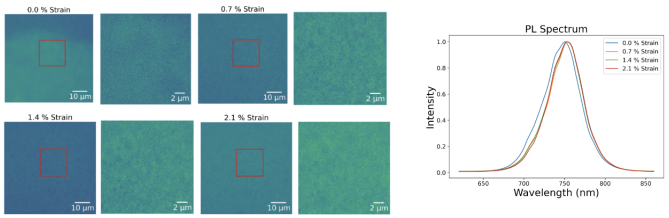

Figure 17. Photobrightening and PL peak shift due to strain.

8. Simulations

8.1. Critical bending radius

The critical bending radius reflects the maximum bending curvature that a PVK can sustain, hence limiting its applications. Here is FEA of the single-crystal perovskite thin film with an NMP design at $R_{bending} = 2.5\,\text{mm}$ [9], [16], [27], [32], [42], [43], [53]

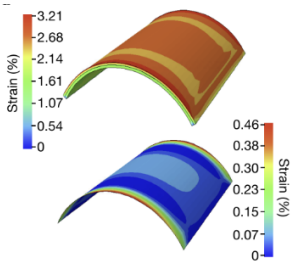

Figure 18. Concave and convex bending strains in a perovskite solar cell.

$K = \Psi\sigma_i c_0^{0.5} > K_{IC} = \sqrt{G_C E}$, where $\Psi = \sqrt{\pi}$, c_0 is the half length of the initial crack;

$R \leq \sqrt{\frac{E}{G_C}} \cdot \frac{\Psi c_0^{0.5}}{2} = R_c$, where R_c is the critical bending radius; the smaller it is, the better.

$\sigma_{\text{net}} = \sigma_R + \sigma_T$, where σ_R is the residual stress due to the difference between the thermal expansion coefficients [1], [51]

8.2. Modelling car surface and extracting its curvature

The car surface was modelled in CAD (Autodesk Computer-Aided Design programme) without wheels for simplification. A program to read any .STL or .OBJ file was created, because those extensions describe best models created either in CAD or Modelo. These were then read in Matlab, and to ensure that it reads the CAD files correctly I printed out the amount of vertices of the car surface, which was somewhat close to my expectation and can be seen on Figure 19.

It is obvious that the car surface is not flat, so it will have curvature at all points. This induces strain within the perovskite, hence affecting the overall performance of the solar cell.

Using the literature review, experimental results and previous models, we are now aiming to optimise the flexible halide perovskites optoelectronic properties by tuning halide ion concentration.

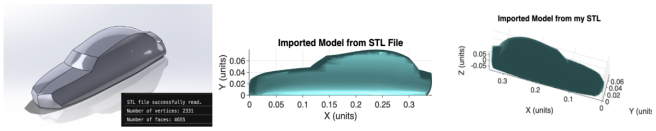

Figure 19. Analysing the CAD car surface and mapping in in Matlab.

When extracting the curvature from the car surface document, Gaussian curvature was chosen, as it is measured with reference to a flat plane. This determines the strains due to the bending of the material. It is also helpful that this curvature is direction-dependent.

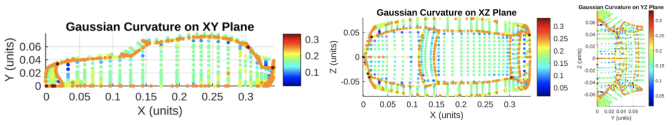

Figure 20. CAD car surface model: extracting the curvature.

To ensure that the perovskite can handle the bending-induced strains, we confirmed radius of the curvature is less than the critical being radius.

Simulations in Matlab using PDE and FEA were conducted to analyze strain distribution based on 3-point bend test.

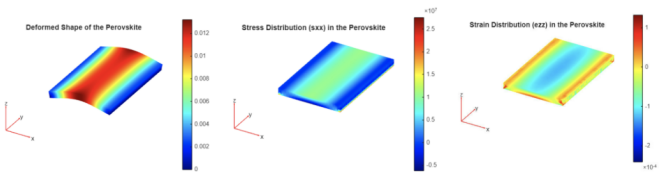

Figure 21. Strains distribution within the perovskite layer.

8.3. Mapping the optoelectronic properties

The next step was assigning a value of an optoelectronic property at a given point within the car surface. This was done by calculating the PVK optoelectronic property in relation to the strain induced by the bending curvature of the car surface.

1. Bandgap energy:

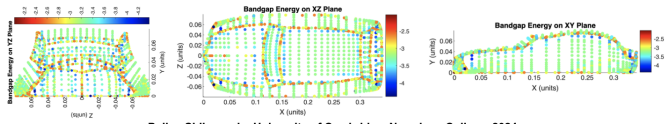

Figure 22. Bandgap energy and curvature.

2. Charge Carrier mobility:

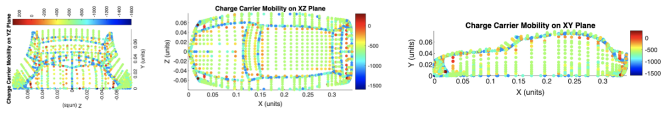

Figure 23. Charge carrier mobility and curvature.

3. Thermal conductivity:

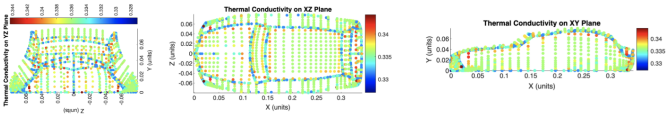

Figure 24. Thermal conductivity and curvature.

We now know how the optoelectronic properties of a perovskite got affected by strain induced by the surface. These are different from original/ optimal values, so we need to optimise them.

8.4. Optimising the optoelectronic properties

3-D plots were chosen to see how much the properties were offset from the ideal values due to applied bending curvature.

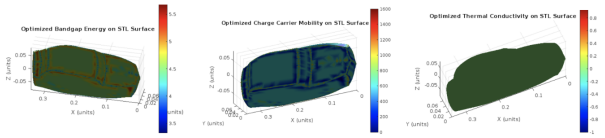

Figure 25. Optimised optoelectronic properties mapped to the car surface.

We use this change to see how much we need to change the halide ion concentration within the perovskite to bring the optoelectronic property either back to its original value or tune it to its optimum.

8.5. Accounting for the change in optoelectronic properties by tuning halide concentration

We have then brought the optoelectronic properties to their needed value by changing the halide ion concentration. This can be seen through the diagrams below.

1. Optimised bandgap energy:

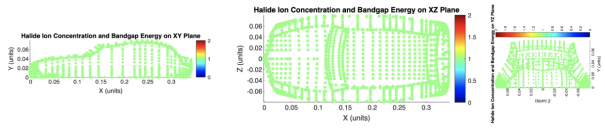

Figure 26. Tuned halide ion concentration to account for changes in bandgap energy.

2. Optimised charge carrier mobility:

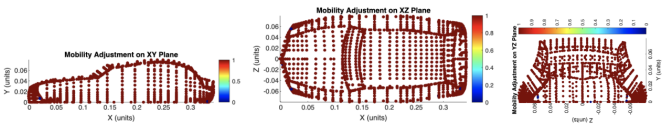

Figure 27. Tuned halide ion concentration to account for changes in charge carrier mobility.

3. Optimised thermal conductivity:

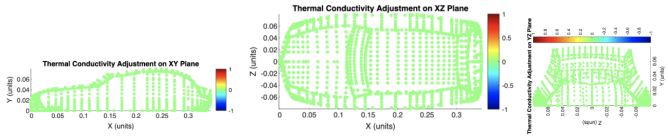

Figure 28. Tuned halide ion concentration to account for changes in thermal conductivity.

4. The final model (3D graphs summary):

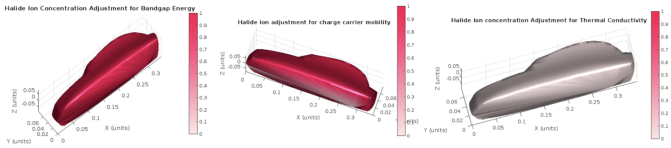

Figure 29. The final model for accounting for the change in optoelectronic properties with halide ion concentration.

Then, we extracted the needed halide ion concentration from figures 26, 27, and 28 to find the new halide ion composition required. Hence, the final model mapping the halide ion concentration to the position within the car surface was created (Figure 28).

8.6. Strain compensation strategies

- The top functional layer should have a higher thermal expansion coefficient than PVK [15, 32].
- The functional layer should interact strongly with the PVK to anchor to the lattice and achieve strain offset [12, 22].
- Strain engineering can be achieved using nanowires [12, 22].
- To account for residual compressive strain, we introduce a tensile strain in the hole transport layer (HTL). By using an HTL with a high thermal expansion coefficient, we compensate for the tensile strain in PSCs by elevating the processing temperature of the HTL [22, 50].
- To stabilize PVK when bending, grain boundary cementation should be considered by adding s-GO (such as adding s-Go to a perovskite to tighten the grain boundaries, much like cement holds the bricks. While nothing to do with actual cement, Xiaotian Hu et al. refer to it this way) [50].
- Bending cycles were tested to make perovskite solar cells more durable and reusable. Devices modified with DT and MoS_2 fully recovered their efficiency after 300 bending cycles, while standard devices only retained 50%.
- A low-temperature process using a 20 nm-thick TiOx or TCO layer improves the efficiency and durability of PSCs [2, 30, 32].

9. Conclusion

Strain optimises the stability of perovskite and, hence, can be used to make the car surface more stable. Internal strain engineering helps in reducing degradation by removing defects [12].

This research underscores the critical role of strain engineering in optimizing the stability and performance of perovskite solar cells (PSCs) on curved surfaces, such as vehicle exteriors. Through extensive modelling and simulations, the impact of bending curvature on the optoelectronic properties of lead-based perovskites was predicted. The accuracy was assessed through comparing our computational results to the experimental ones.

Finite Element Analysis (FEA) and Partial Differential Equation (PDE) simulations allowed for precise calculations of strain distribution across the PSC layers, showing the relationship between compressive strain and enhanced charge carrier mobility and thermal conductivity. Conversely, the tensile strain was shown to degrade these properties, highlighting the anisotropic behaviour of perovskites under mechanical stress.

The research stresses the importance of measuring the change in optoelectronic properties in major crystallographic axes; otherwise, the results are incomplete due to perovskites' anisotropy. The findings underscore the importance of substrate choice and strain compensation strategies in maintaining mechanical reliability and enhancing the efficiency of PSCs on non-flat surfaces, such as those found on vehicles. By leveraging strain engineering and compositional tuning, it is possible to develop more durable and efficient PSCs, paving the way for their integration into next-generation automotive applications.

10. Limitations and future work

Due to the unstable nature of PVKs, it might not be possible to change the halide ion concentration enough to fully offset the change in optoelectronic properties due to halide ion segregation. Furthermore, there might also be separation between the cations. due to light and ion migration. Ultimately, we should look into PVK end-of-life-cycle applications.

It would be useful to continue the investigation for thin films too, as the PVK car surface would consist of those due to their lower costs, and that it is easier to grow a thin film than a single crystal o a sufficient size. Taking this further, scalability and manufacturing shall be evaluated too.

Ultimately, the data was extracted using computer vision, so there might be a discrepancy between the values presented here and the actual values on the graphs.

11. Acknowledgements

I am deeply grateful to Dr. Claire Barlow for supervising this project, reviewing both the report and the poster and ensuring that I actually get things done.

I am thankful to Dr Miloš Dubajić and Capucine Mamak for helping with the measurements, explaining hyperspectral imaging, and then growing the crystals. Additionally, I appreciate Gregg Chu's input on the substrates (despite the fact that I thought the OHP substrate was a file), and Aldric Goh and Dr Stephanie Adeyemo for introducing me to THz and helping me get started with the project.

12. Supplementary material

All of the data and preliminary versions are available by following a link to my Laidlaw folder in Google Drive. The car surface analysed in the Simulations section can be found there too.

My code and a method to use it can be found in my GitHub repository. Alternatively, the libraries that I used are presented within the Methodology (Simulations) sections.

The end.

13. References

(1) Sun, S.; Fang, Y.; Kieslich, G.; White, T. J.; Cheetham, A. K. Mechanical Properties of Organic–Inorganic Halide Perovskites, CH 3 NH 3 PbX 3 (X = I, Br and Cl), by Nanoindentation. J. Mater. Chem. A 2015, 3 (36), 18450–18455. https://doi.org/10.1039/C5TA03331D.

(2) Karimipour, M.; Khazraei, S.; Kim, B. J.; Boschloo, G.; Johansson, E. M. J. Efficient and Bending Durable Flexible Perovskite Solar Cells via Interface Modification Using a Combination of Thin MoS2 Nanosheets and Molecules Binding to the Perovskite. Nano Energy 2022, 95, 107044. https://doi.org/10.1016/j.nanoen.2022.107044.

(3) Instruments, E. Measuring the Carrier Lifetime of Perovskites Using Time-Resolved Photoluminescence. 2020, 35, 69–69.

(4) Wu, J.; Liu, S.-C.; Li, Z.; Wang, S.; Xue, D.-J.; Lin, Y.; Hu, J.-S. Strain in Perovskite Solar Cells: Origins, Impacts and Regulation. National Science Review 2021, 8 (8), nwab047. https://doi.org/10.1093/nsr/nwab047.

(5) Witkoske, E.; Tong, Z.; Feng, Y.; Ruan, X.; Lundstrom, M.; Lu, N. The Use of Strain and Grain Boundaries to Tailor Phonon Transport Properties: A First-Principles Study of 2H-Phase CuAlO2. II. Journal of Applied Physics 2020, 127 (11), 115108. https://doi.org/10.1063/1.5142485.

(6) Revealing the strain-associated physical mechanisms impacting the performance and stability of perovskite solar cells - ScienceDirect. https://www.sciencedirect.com/science/article/pii/S2542435122000435 (accessed 2024-07-29).

(7) Moloney, E. G.; Yeddu, V.; Saidaminov, M. I. Strain Engineering in Halide Perovskites. ACS Materials Lett. 2020, 2 (11), 1495–1508. https://doi.org/10.1021/acsmaterialslett.0c00308.

(8) Prasanna, R.; Gold-Parker, A.; Leijtens, T.; Conings, B.; Babayigit, A.; Boyen, H.-G.; Toney, M. F.; McGehee, M. D. Band Gap Tuning via Lattice Contraction and Octahedral Tilting in Perovskite Materials for Photovoltaics. J. Am. Chem. Soc. 2017, 139 (32), 11117–11124. https://doi.org/10.1021/jacs.7b04981.

(9) Wei, R. Modelling of Perovskite Solar Cells.

(10) Bouhmouche, A.; Jabar, A.; Natik, A.; Lassri, H.; Abid, M.; Moubah, R. Strain Engineering on the Optoelectronic Properties of CsPbI3 Halide Perovskites: Ab-Initio Investigation. J. Electron. Mater. 2023, 52 (8), 5430–5439. https://doi.org/10.1007/s11664-023-10476-w.

(11) Haeger, T.; Heiderhoff, R.; Riedl, T. Thermal Properties of Metal-Halide Perovskites. J. Mater. Chem. C 2020, 8 (41), 14289–14311. https://doi.org/10.1039/D0TC03754K.

(12) Attique, S.; Ali, N.; Imran, T.; Rauf, S.; Khesro, A.; Ali, S.; Wang, W.; Khatoon, R.; Abbas, A.; Ullah khan, E.; Yang, S.; Wu, H. An Overview of the Pressure- and Strain-Induced Changes in the Structural and Optoelectronic Properties of Organometal Halide Perovskites. Solar Energy 2022, 239, 198–220. https://doi.org/10.1016/j.solener.2022.05.009.

(13) Islam, R.; Liu, K.; Wang, Z.; Hasan, S.; Wu, Y.; Qu, S.; Wang, Z. Strain-Induced Electronic and Optical Properties of Inorganic Lead Halide Perovskites APbBr3 (A= Rb and Cs). Materials Today Communications 2022, 31, 103305. https://doi.org/10.1016/j.mtcomm.2022.103305.

(14) Li, Z.; Wang, X.; Wang, Z.; Shao, Z.; Hao, L.; Rao, Y.; Chen, C.; Liu, D.; Qiangqiang, Z.; Sun, X.; Gao, C.; Zhang, B.; Wang, X.; Wang, L.; Cui, G.; Pang, S. Ammonia for Post-Healing of Formamidinium-Based Perovskite Films. Nature Communications 2022, 13. https://doi.org/10.1038/s41467-022-32047-z.

(15) Courtier, N. E.; Cave, J. M.; Foster, J. M.; Walker, A. B.; Richardson, G. How Transport Layer Properties Affect Perovskite Solar Cell Performance: Insights from a Coupled Charge Transport/Ion Migration Model. Energy Environ. Sci. 2019, 12 (1), 396–409. https://doi.org/10.1039/C8EE01576G.

(16) Ekuma, C. Computational Synthesis of a New Generation of 2D-Based Perovskite Quantum Materials. APL Machine Learning 2024, 2. https://doi.org/10.1063/5.0189497.

(17) Rong, S.-S.; Faheem, M. B.; Li, Y.-B. Perovskite Single Crystals: Synthesis, Properties, and Applications. Journal of Electronic Science and Technology 2021, 19 (2), 100081. https://doi.org/10.1016/j.jnlest.2021.100081.

(18) Cao, S.; Su, Y.; Song, K.-K.; Qian, P.; Yan, Y.; Shi, L.-B. Biaxial Strain Improving Carrier Mobility for Inorganic Perovskite: Ab Initio Boltzmann Transport Equation. J. Phys.: Condens. Matter 2022, 35 (5), 055702. https://doi.org/10.1088/1361-648X/aca3eb.

(19) Alqahtani, S. M.; Alsayoud, A. Q.; Alharbi, F. H. Structures, Band Gaps, and Formation Energies of Highly Stable Phases of Inorganic ABX3 Halides: A = Li, Na, K, Rb, Cs, Tl; B = Be, Mg, Ca, Ge, Sr, Sn, Pb; and X = F, Cl, Br, I. RSC Adv 13 (13), 9026–9032. https://doi.org/10.1039/d3ra00185g.

(20) Liu, D.; Luo, D.; Iqbal, A. N.; Orr, K. W. P.; Doherty, T. A. S.; Lu, Z.-H.; Stranks, S. D.; Zhang, W. Strain Analysis and Engineering in Halide Perovskite Photovoltaics. Nat. Mater. 2021, 20 (10), 1337–1346. https://doi.org/10.1038/s41563-021-01097-x.

(21) Zhu, C.; Niu, X.; Fu, Y.; Li, N.; Hu, C.; Chen, Y.; He, X.; Na, G.; Liu, P.; Zai, H.; Ge, Y.; Lu, Y.; Ke, X.; Bai, Y.; Yang, S.; Chen, P.; Li, Y.; Sui, M.; Zhang, L.; Zhou, H.; Chen, Q. Strain Engineering in Perovskite Solar Cells and Its Impacts on Carrier Dynamics. Nat Commun 2019, 10 (1), 815. https://doi.org/10.1038/s41467-019-08507-4.

(22) Xue, D.-J.; Hou, Y.; Liu, S.-C.; Wei, M.; Chen, B.; Huang, Z.; Li, Z.; Sun, B.; Proppe, A. H.; Dong, Y.; Saidaminov, M. I.; Kelley, S. O.; Hu, J.-S.; Sargent, E. H. Regulating Strain in Perovskite Thin Films through Charge-Transport Layers. Nat Commun 2020, 11 (1), 1514. https://doi.org/10.1038/s41467-020-15338-1.

(23) Yadav, K.; Ray, N. Assessing the Impact of Triaxial Strain on Carrier Mobility and Dielectric Properties in Cubic CsBCl3 (B = Pb, Sn, or Ge) Perovskites: A First Principles Study. AIP Advances 2023, 13 (12), 125304. https://doi.org/10.1063/5.0181531.

(24) Shai, X.; Chen, W.; Sun, J.; Liu, J.; Chen, J. Origins, Impacts, and Mitigation Strategies of Strain in Efficient and Stable Perovskite Solar Cells. Small Science 2023, 3 (7), 2300014. https://doi.org/10.1002/smsc.202300014.

(25) Liu, K.; Wang, Z.; Qu, S.; Ding, L. Stress and Strain in Perovskite/Silicon Tandem Solar Cells. Nanomicro Lett 2023, 15, 59. https://doi.org/10.1007/s40820-023-01019-3.

(26) Handa, T.; Yamada, T.; Nagai, M.; Kanemitsu, Y. Phonon, Thermal, and Thermo-Optical Properties of Halide Perovskites. Phys. Chem. Chem. Phys. 2020, 22 (45), 26069–26087. https://doi.org/10.1039/D0CP04426A.

(27) Li, Y.; Lu, Y.; Huo, X.; Wei, D.; Meng, J.; Dong, J.; Qiao, B.; Zhao, S.; Xu, Z.; Song, D. Bandgap Tuning Strategy by Cations and Halide Ions of Lead Halide Perovskites Learned from Machine Learning. RSC Advances 2021, 11 (26), 15688–15694. https://doi.org/10.1039/D1RA03117A.

(28) Kumawat, N. K.; Dey, A.; Kumar, A.; Gopinathan, S. P.; Narasimhan, K. L.; Kabra, D. Band Gap Tuning of CH3NH3Pb(Br1–XClx)3 Hybrid Perovskite for Blue Electroluminescence. ACS Appl. Mater. Interfaces 2015, 7 (24), 13119–13124. https://doi.org/10.1021/acsami.5b02159.

(29) Tablero Crespo, C. The Effect of the Halide Anion on the Optical Properties of Lead Halide Perovskites. Solar Energy Materials and Solar Cells 2019, 195, 269–273. https://doi.org/10.1016/j.solmat.2019.03.023.

(30) Pisoni, S.; Carron, R.; Moser, T.; Feurer, T.; Fu, F.; Nishiwaki, S.; Tiwari, A. N.; Buecheler, S. Tailored Lead Iodide Growth for Efficient Flexible Perovskite Solar Cells and Thin-Film Tandem Devices. NPG Asia Mater 2018, 10 (11), 1076–1085. https://doi.org/10.1038/s41427-018-0099-1.

(31) Liang, H.; Yang, W.; Xia, J.; Gu, H.; Meng, X.; Yang, G.; Fu, Y.; Wang, B.; Cai, H.; Chen, Y.; Yang, S.; Liang, C. Strain Effects on Flexible Perovskite Solar Cells. Advanced Science 2023, 10 (35), 2304733. https://doi.org/10.1002/advs.202304733.

(32) Kim, B. J.; Kim, D. H.; Lee, Y.-Y.; Shin, H.-W.; Han, G. S.; Hong, J. S.; Mahmood, K.; Ahn, T. K.; Joo, Y.-C.; Hong, K. S.; Park, N.-G.; Lee, S.; Jung, H. S. Highly Efficient and Bending Durable Perovskite Solar Cells: Toward a Wearable Power Source. Energy Environ. Sci. 2015, 8 (3), 916–921. https://doi.org/10.1039/C4EE02441A.

(33) Meng, W.; Zhang, K.; Osvet, A.; Zhang, J.; Gruber, W.; Forberich, K.; Meyer, B.; Heiss, W.; Unruh, T.; Li, N.; Brabec, C. J. Revealing the Strain-Associated Physical Mechanisms Impacting the Performance and Stability of Perovskite Solar Cells. Joule 2022, 6 (2), 458–475. https://doi.org/10.1016/j.joule.2022.01.011.

(34) Lam, D. UNDERSTANDING THE ROLE OF CHARGE MOBILITY AND RECOMBINATION IN ORGANIC PHOTOVOLTAICS.

(35) Saliba, M.; Matsui, T.; Seo, J.-Y.; Domanski, K.; Correa-Baena, J.-P.; Nazeeruddin, M. K.; Zakeeruddin, S. M.; Tress, W.; Abate, A.; Hagfeldt, A.; Grätzel, M. Cesium-Containing Triple Cation Perovskite Solar Cells: Improved Stability, Reproducibility and High Efficiency. Energy Environ. Sci. 2016, 9 (6), 1989–1997. https://doi.org/10.1039/C5EE03874J.

(36) Orr, K. Strain in Halide Perovskites: Characterisation, Crystallography, Consequences. 2024. https://doi.org/10.17863/CAM.108243.

(37) Yang, B.; Bogachuk, D.; Suo, J.; Wagner, L.; Kim, H.; Lim, J.; Hinsch, A.; Boschloo, G.; Nazeeruddin, M. K.; Hagfeldt, A. Strain Effects on Halide Perovskite Solar Cells. Chem. Soc. Rev. 2022, 51 (17), 7509–7530. https://doi.org/10.1039/D2CS00278G.

(38) Lafalce, E.; Amerling, E.; Yu, Z.-G.; Sercel, P. C.; Whittaker-Brooks, L.; Vardeny, Z. V. Rashba Splitting in Organic–Inorganic Lead–Halide Perovskites Revealed through Two-Photon Absorption Spectroscopy. Nat Commun 2022, 13 (1),

483. https://doi.org/10.1038/s41467-022-28127-9.

(39) Zeng, X.; Niu, G.; fg, X.; Jiang, J.; Sui, L.; Zhang, Y.; Chen, A.; Jin, M.; Yuan, K.; Yang, X. Enhanced Carrier Transport in CsxSnBry Perovskite by Reducing Electron-Phonon Coupling under Compressive Strain. Materials Today Physics 2024, 40, 101296. https://doi.org/10.1016/j.mtphys.2023.101296.

(40) Wang, G.; Fan, H.; Chen, Z.; Gao, Y.; Wang, Z.; Li, Z.; Lu, H.; Zhou, Y. Tuning Thermal Conductivity of Hybrid Perovskites through Halide Alloying. Advanced Science 2024, 11 (25), 2401194. https://doi.org/10.1002/advs.202401194.

(41) Modelo. https://app.modelo.io/damf/model/3FO4K8GEQXDC (accessed 2024-07-21).

(42) Workman, M.; Chen, D. Z.; Musa, S. M. Csx MA1-x Pb(I1-x Brx)3 Perovskite Solar Cell Fabrication and Modeling. In 2020 International Conference on Technology and Policy in Energy and Electric Power (ICT-PEP); 2020; pp 116–120. https://doi.org/10.1109/ICT-PEP50916.2020.9249794.

(43) Lei, Y.; Chen, Y.; Zhang, R.; Li, Y.; Yan, Q.; Lee, S.; Yu, Y.; Tsai, H.; Choi, W.; Wang, K.; Luo, Y.; Gu, Y.; Zheng, X.; Wang, C.; Wang, C.; Hu, H.; Li, Y.; Qi, B.; Lin, M.; Zhang, Z.; Dayeh, S. A.; Pharr, M.; Fenning, D. P.; Lo, Y.-H.; Luo, J.; Yang, K.; Yoo, J.; Nie, W.; Xu, S. A Fabrication Process for Flexible Single-Crystal Perovskite Devices. Nature 2020, 583 (7818), 790–795. https://doi.org/10.1038/s41586-020-2526-z.

(44) Strain Engineering of Metal Halide Perovskites on Coupling Anisotropic Behaviors - Jiao - 2021 - Advanced Functional Materials - Wiley Online Library. https://onlinelibrary.wiley.com/doi/abs/10.1002/adfm.202006243 (accessed 2024-07-27).

(45) Strain Engineering in Perovskites: Mutual Insight on Oxides and Halides - Choi - 2024 - Advanced Materials - Wiley Online Library. https://onlinelibrary.wiley.com/doi/abs/10.1002/adma.202308827 (accessed 2024-07-27).

(46) Courtier, N. E.; Cave, J. M.; Walker, A. B.; Richardson, G.; Foster, J. M. IonMonger: A Free and Fast Planar Perovskite Solar Cell Simulator with Coupled Ion Vacancy and Charge Carrier Dynamics. J Comput Electron 2019, 18 (4), 1435–1449. https://doi.org/10.1007/s10825-019-01396-2.

(47) Pei, L.; Yu, H.; Zhang, Q.; Li, J.; Wang, K.; Hu, B. Concave and Convex Bending Influenced Mechanical Stability in Flexible Perovskite Solar Cells. J. Phys. Chem. C 2020, 124 (4), 2340–2345. https://doi.org/10.1021/acs.jpcc.9b10407.

(48) Kim, J.-H.; Lee, I.; Kim, T.-S.; Rolston, N.; Watson, B. L.; Dauskardt, R. H. Understanding Mechanical Behavior and Reliability of Organic Electronic Materials. MRS Bulletin 2017, 42 (2), 115–123. https://doi.org/10.1557/mrs.2017.3.

(49) Jung, H. S.; Han, G. S.; Park, N.-G.; Ko, M. J. Flexible Perovskite Solar Cells. Joule 2019, 3 (8), 1850–1880. https://doi.org/10.1016/j.joule.2019.07.023.

(50) Hu, X.; Meng, X.; Yang, X.; Huang, Z.; Xing, Z.; Li, P.; Tan, L.; Su, M.; Li, F.; Chen, Y.; Song, Y. Cementitious Grain-Boundary Passivation for Flexible Perovskite Solar Cells with Superior Environmental Stability and Mechanical Robustness. Science Bulletin 2021, 66 (6), 527–535. https://doi.org/10.1016/j.scib.2020.10.023.

(51) Mechanical study of perovskite solar cells: opportunities and challenges for wearable power source. https://opg.optica.org/ome/fulltext.cfm?uri=ome-12-2-772id=468895 (accessed 2024-06-26).

(52) Wang, Y.; Sui, R.; Bi, M.; Tang, W.; Ma, S. Strain Sensitivity of Band Structure and Electron Mobility in Perovskite BaSnO 3: First-Principles Calculation. RSC Advances 2019, 9 (25), 14072–14077. https://doi.org/10.1039/C9RA02146A.

(53) Teixeira, C. O.; Castro, D.; Andrade, L.; Mendes, A. Selection of the Ultimate Perovskite Solar Cell Materials and Fabrication Processes towards Its Industrialization: A Review. Energy Science Engineering 2022, 10 (4), 1478–1525. https://doi.org/10.1002/ese3.1084.

(54) Anharmonicity and Ultra-Low Thermal Conductivity in Lead-Free Halide Double Perovskites. https://ar5iv.labs.arxiv.org/html/1912.05351 (accessed 2024-07-30).

(55) Cheng, R.; Zeng, Z.; Wang, C.; Ouyang, N.; Chen, Y. Impact of Strain-Insensitive Low-Frequency Phonon Modes on Lattice Thermal Transport in A_2XB_6-Type Perovskites. Phys. Rev. B 2024, 109 (5), 054305. https://doi.org/10.1103/PhysRevB.109.054305.

(56) Kim, H. D.; Ohkita, H. Potential Improvement in Fill Factor of Lead-Halide Perovskite Solar Cells. Sol. RRL 2017, 1 (6), 1700027. https://doi.org/10.1002/solr.201700027..

(57) Short-Circuit Current | PVEducation. https://www.pveducation.org/pvcdrom/solar-cell-operation/short-circuit-current (accessed 2024-07-30).

(58) Helal Miah, M.; Uddin Khandaker, M.; Bulu Rahman, M.; Nur-E-Alam, M.; Aminul Islam, M. Band Gap Tuning of Perovskite Solar Cells for Enhancing the Efficiency and Stability: Issues and Prospects. RSC Advances 2024, 14 (23), 15876–15906. https://doi.org/10.1039/D4RA01640H.

(59) Nelson, J. A. The Physics of Solar Cells; Imperial College Press: Singapore, SINGAPORE, 2003.

(60) Herz, L. M. Charge-Carrier Mobilities in Metal Halide Perovskites: Fundamental Mechanisms and Limits. ACS Energy Lett. 2017, 2 (7), 1539–1548. https://doi.org/10.1021/acsenergylett.7b00276.

(61) Jing, H.; Sa, R.; Xu, G. Tuning Electronic and Optical Properties of CsPbI3 by Applying Strain: A First-Principles Theoretical Study. Chemical Physics Letters 2019, 732, 136642. https://doi.org/10.1016/j.cplett.2019.136642.

(62) gmp007. Gmp007/Perovskene-Materials, 2024. https://github.com/gmp007/perovskene-materials (accessed 2024-08-02).

(63) PerovskiteSCModelling/IonMonger, 2024. https://github.com/PerovskiteSCModelling/IonMonger (accessed 2024-08-02).

(64) Chen, X.; Kamat, P. V.; Janáky, C.; Samu, G. F. Charge Transfer Kinetics in Halide Perovskites: On the Constraints of Time-Resolved Spectroscopy Measurements. ACS Energy Lett. 2024, 9 (6), 3187–3203. https://doi.org/10.1021/acsenergylett.4c00736.

(65) Yuan, Y.; Yan, G.; Dreessen, C.; Rudolph, T.; Hülsbeck, M.; Klingebiel, B.; Ye, J.; Rau, U.; Kirchartz, T. Shallow Defects

and Variable Photoluminescence Decay Times up to 280 s in Triple-Cation Perovskites. Nat. Mater. 2024, 23 (3), 391–397. https://doi.org/10.1038/s41563-023-01771-2.

(66) Kanemitsu, Y.; Yamada, T.; Handa, T.; Nagai, M. Optical Responses of Lead Halide Perovskite Semiconductors. Semicond. Sci. Technol. 2020, 35 (9), 093001. https://doi.org/10.1088/1361-6641/ab95b1.

(67) Zhang, L.; Geng, W.; Tong, C.-J.; Chen, X.; Cao, T.; Chen, M. Strain Induced Electronic Structure Variation in Methyl-Ammonium Lead Iodide Perovskite. Sci Rep 2018, 8 (1), 7760. https://doi.org/10.1038/s41598-018-25772-3.

(68) cmd-l. Cmd-l/ComputationalMaterialsScreening, 2023. https://github.com/cmd-l/ComputationalMaterialsScreening (accessed 2024-08-10).

(69) Akkerman, Q. A.; Manna, L. What Defines a Halide Perovskite? ACS Energy Lett 2020, 5 (2), 604–610. https://doi.org/10.1021/acsenergylett.0c00039.

(70) Jiao, Y.; Ma, F.; Wang, H.; Bell, J.; Du, A. Strain Mediated Bandgap Reduction, Light Spectrum Broadening, and Carrier Mobility Enhancement of Methylammonium Lead/Tin Iodide Perovskites. Particle and Particle Systems Characterization 2017, 34 (4), 1600288. https://doi.org/10.1002/ppsc.201600288.

(71) Dam, S. Stress-Induced Optoelectronic Changes in Thin Film Solar Cells. AZoM. https://www.azom.com/news.aspx?newsID=60375 (accessed 2024-08-11).

(72) Bending moments and beam curvatures. https://www.doitpoms.ac.uk/tlplib/beambending/bendmoments.php (accessed 2024-08-11).

(73) Chen, Y.; Lei, Y.; Li, Y.; Yu, Y.; Cai, J.; Chiu, M.-H.; Rao, R.; Gu, Y.; Wang, C.; Choi, W.; Hu, H.; Wang, C.; Li, Y.; Song, J.; Zhang, J.; Qi, B.; Lin, M.; Zhang, Z.; Islam, A. E.; Maruyama, B.; Dayeh, S.; Li, L.-J.; Yang, K.; Lo, Y.-H.; Xu, S. Strain Engineering and Epitaxial Stabilization of Halide Perovskites. Nature 2020, 577 (7789), 209–215. https://doi.org/10.1038/s41586-019-1868-x.

(74) Terahertz Spectroscopy of Emerging Materials | The Journal of Physical Chemistry C. https://pubs.acs.org/doi/abs/10.1021/acs.jpcc.0c06344 (accessed 2024-08-11).

(75) Koch, M.; Mittleman, D. M.; Ornik, J.; Castro-Camus, E. Terahertz Time-Domain Spectroscopy. Nat Rev Methods Primers 2023, 3 (1), 48. https://doi.org/10.1038/s43586-023-00232-z.

(76) Joyce, H. J.; Boland, J. L.; Davies, C. L.; Baig, S. A.; Johnston, M. B. A Review of the Electrical Properties of Semiconductor Nanowires: Insights Gained from Terahertz Conductivity Spectroscopy. Semicond. Sci. Technol. 2016, 31 (10), 103003. https://doi.org/10.1088/0268-1242/31/10/103003.

(77) Chen, L.; Adeyemo, S. O.; Fonseka, H. A.; Liu, H.; Kar, S.; Yang, H.; Velichko, A.; Mowbray, D. J.; Cheng, Z.; Sanchez, A. M.; Joyce, H. J.; Zhang, Y. Long-Term Stability and Optoelectronic Performance Enhancement of InAsP Nanowires with an Ultrathin InP Passivation Layer. Nano Lett. 2022, 22 (8), 3433–3439. https://doi.org/10.1021/acs.nanolett.2c00805.

(78) Petsiuk, A. Untersuchung Des Ladungstransportes in Den Metal Halogenid Perowskiten Durch THz SpektroskopieInvestigation of Charge Carrier Transport in Metal Halide Perovskites by THz Spectroscopy, Universität Potsdam, 2021, p 2768 KB, 118 pages. https://doi.org/10.25932/PUBLISHUP-51544.

(79) Momma, K.; Izumi, F. VESTA 3 for Three-Dimensional Visualization of Crystal, Volumetric and Morphology Data. J Appl Cryst 2011, 44 (6), 1272–1276. https://doi.org/10.1107/S0021889811038970.